Journal of Computational Physics 228 (2009) 5710–5721

Contents lists available at ScienceDirect

Journal of Computational Physics

journal homepage: www.elsevier.com/locate/jcp

Crack reconstruction using a level-set strategy

Diego Álvarez *, Oliver Dorn, Natalia Irishina, Miguel Moscoso

Gregorio Millán Institute, Universidad Carlos III de Madrid, Avenida de la Universidad 30, 28911 Leganés, Spain

ARTICLE INFO

Article history:
Received 21 October 2008
Received in revised form 24 March 2009
Accepted 17 April 2009
Available online 6 May 2009

PACS:
02.30.Zz
42.30.Wb
41.20.Cv

Keywords:
Electrical impedance tomography
Level-sets
Crack reconstruction

ABSTRACT

We present a level-set based technique to recover key characteristics of a defect or crack (e.g. location, length and shape) in a two-dimensional material from boundary electrical measurements. The key feature of this work is to extend the usual level-set technique for modeling volumetric objects to very thin objects. Two level-set functions are employed: the first one models the location and form of the crack, and the second one models its length and connectivity. An efficient gradient based method is derived in order to define evolution laws for these two level-set functions which minimize the least squares data misfit. Numerical experiments show the utility of this method even in the presence of a significant noise level in the measurements. A finite element method is used to simulate the electric field behavior in the presence of very thin objects.

1. Introduction

The problem of determining the location, size and shape of flaws within a material from measurements on its surface is of much interest in non-destructive testing. This is an important problem from the computational, medical and industrial viewpoints. Boundary data can be obtained from thermal, acoustic, elastostatic, or electrostatic measurements, amongst others. For example, Friedman and Vogelius [22] initiated these studies for a steady state thermal problem and proved uniqueness for a single buried crack under some conditions; Liepa et al. [30] used electrical measurements to determine the location and size of a straight-line crack; Kress [27] considered the time-harmonic acoustic inverse problem for a sound-soft crack (or perfectly conducting) in $\mathbb{R}^2$. He extended this work also to the case of elastic wave scattering from a thin infinitely long cylindrical crack in [28].

As a model problem, we consider here a two-dimensional material Ω in which electric currents are created by applying voltage potentials γ_j at its boundary. By doing so, the electric potential u_j satisfies

$$\nabla \cdot b(\mathbf{x})\nabla u_j = 0 \quad \text{in } \Omega \tag{1}$$

and

$$u_j = \gamma_j \quad \text{on } \partial\Omega. \tag{2}$$

The voltages are applied at different points at the boundary in order to create sufficient diversity in the data.

* Corresponding author. Tel.: +34 91 624 88 24; fax: +34 91 624 91 29.
E-mail addresses: jdiego@math.uc3m.es (D. Álvarez), odorn@math.uc3m.es (O. Dorn), nirishin@math.uc3m.es (N. Irishina), moscoso@math.uc3m.es (M. Moscoso).

0021-9991/$ - see front matter © 2009 Elsevier Inc. All rights reserved.
doi:10.1016/j.jcp.2009.04.038

We are interested in the case where the conductivity profile $b(\mathbf{x})$ contains sharp discontinuities between the background material and a crack-like shape. Without loss of generality, we consider in this paper thin insulating cracks with a finite contrast in conductivity between the interior and the exterior of the crack, i.e., we model the cracks as very thin structures with a small and fixed thickness along the crack. The location, form and connectivity structure of the cracks is unknown, which means that the crack could consist of two (or more) different parts which are disconnected. The electrical properties in the whole domain are piecewise constant with only two possible values (referring to the interior and the exterior of the crack) which are known a priori. We assume that the electrical properties inside the crack region are sufficiently different from the background material. Therefore, our problem is an inverse crack problem related to electrical impedance tomography [24,8,15,9].

Regardless of the kind of measurements taken at the boundary, many different inversion approaches have been applied in the literature so far to detect the presence of a crack and to determine its location and size. Overall, we can distinguish two classes of methods: non-iterative methods and iterative methods.

Non-iterative methods, such as the reciprocity gap technique for straight-line cracks [3,2] or the factorization method [10], are fast but generally do not provide detailed information about the crack. Baratchart et al. [5] introduced a meromorphic approximation approach to solve some 2D inverse problems for the Laplacian. Even though this method only requires one numerical experiment, it can only locate the end points of the crack.

On the other hand, iterative methods are computationally more expensive. They need to solve a direct problem at each step to compute the Fréchet derivative of the underlying forward operator, but they usually offer very accurate results (provided that a good initial estimate of the crack is used). These methods have been studied extensively over the last two decades. Among these methods, we mention [27,28] where the crack is found from the measured far-field data using a regularized Newton method. Recently, Kress and Serranho [29] proposed a hybrid method to solve the inverse scattering problem for sound-soft cracks in two dimensions. In that work, the authors combine ideas of both, non-iterative and iterative methods. We also want to mention here that sampling methods have been applied to the inverse crack problem [26,13] with success.

For more information regarding the very interesting existing literature on crack detection problems, we refer the reader to consulting the expositions given in [6,7,14,19,32,38], and the further references given there. We also want to mention the recent thesis [36] which presents and compares various techniques for crack detection in non-destructive testing and the related work in [1] which treats cracks in 3D domains by a volumetric level set approach for eddy current imaging.

The main purpose of this paper is to investigate the potential of shape-based reconstruction algorithms that use level-set techniques to recover the location and geometry of a disconnected snake-like crack. Since the seminal work in [39], level-set techniques (originally introduced in [34] for computational front propagation) have been widely used for solving inverse problems with great success [39,31,21,17,12,25,37] (see [18] for a recent overview on level-set techniques applied to inverse problems). However, level-set techniques are intrinsically designed for the case of volumetric objects. If these objects have negligible volume, as is commonly the case in flaws encountered in materials, the standard level-set technique cannot be applied in a straightforward manner. It is our goal here to present one possible extension of the level-set technique for the inverse crack problem. By some appropriate adaptations of classical tools to this new situation, we give evolution laws for an initial guess in both its normal and tangential directions during the iterative process. The evolution of the normal component will correspond to the movement of the crack over the domain, whereas a tangential evolution will affect the length and connectivity of the crack. We present an efficient two-step numerical scheme which during the early iterations intends to reduce the data misfit by considering an evolving straight-line (multi) crack, and during the later iterations intends to find more details of the crack, in particular its curvature at each point. Our technique relies on the assumption that the nonlinear cost functional representing the data misfit can be approximated locally by a linear operator.

We mention that the direct problem of moving a curve using a level-set approach has already been studied by Burchard et al. [11], amongst others. They represent the evolving curve in R^3 by the intersection between the zero level sets of two level-set functions, and they show that their representation automatically handles mergings and breakings of the curve under a variety of geometrically based motions. The motion of curves in R^2 and R^3 is important to model several physical phenomena such as crack growth [42–44,16]. In [42,43], the authors present an algorithm which couples the level-set method with the extended finite element method for modeling propagating cracks. Instead, an element-free Galerkin method is used in [44] with a vector level-set method. Also, a numerical method that couples the extended finite element method to the fast marching method has been proposed in [16]. A review of the different techniques for tracking the motion of a curve by level-set functions can be found in [20].

The paper is organized as follows. In Section 2 we explain our novel approach for representing cracks by a pair of two level-set functions. In Section 3 we state the inverse problem and present the numerical algorithm for the reconstruction of the shapes. In Section 4 we give some technical details about the numerical method, the type of measurements we use, the regularization applied to stabilize the reconstruction process, and other details about the reconstruction algorithm. In Section 5 we show several numerical experiments which demonstrate the performance of our new algorithm. Section 6 contains our conclusions and some hints to future work.

2. Modeling cracks using level-sets

As we have mentioned in the introduction, the current paper is an attempt towards using level-set techniques for reconstructing objects with negligible volume. Our objective is to reconstruct the thin objects (including their connectivity) using

measured data taken on the boundary $\partial\Omega$ of the material. In particular, we are interested in recovering crack-like defects in a homogeneous medium. To this end, we need first to have a tool to represent these thin objects that can handle in a flexible way the shape reconstruction problem. We will adapt here the usual level-set representation for describing volumetric objects to the situation in which these objects are very thin. The advantage of a level-set representation compared to more traditional descriptions of shapes, like parametric representations, is that level-set methods provide an implicit representation of the shapes. This will free us from topological restrictions during the iterative reconstruction of its shape.

Let us assume that we have a continuously differentiable level-set function $\varphi(\mathbf{x}) = \varphi(x,y)$, such that its zero level-set [35,40]

$$\Gamma_\varphi = \{(x,y) \in \Omega : \varphi(x,y) = 0\} \tag{3}$$

specifies a connected curve within Ω (see Fig. 1). The normal $\mathbf{n}$ to Γ_φ will be defined by

$$\mathbf{n}(\mathbf{x}) = \frac{\nabla\varphi}{|\nabla\varphi|} \quad \text{on } \Gamma_\varphi \tag{4}$$

pointing to the region where $\varphi(x,y) \geqslant 0$.

Notice, that so far, we would only be able to represent a single connected crack that, in addition, would reach the boundary $\partial\Omega$, being therefore 'visible' from outside. To circumvent this problem, the authors in [42] represent each endpoint of the crack as the intersection of the zero level set of φ with an orthogonal zero level set of another level-set function (one for each endpoint of the crack). We follow here a slightly different approach presented in [41] to model spiral crystal growth. In this representation, only a second level-set function is necessary regardless of the number of crack tips. This is very important in our problem since the initial crack may break into several pieces during the reconstruction process, and therefore the number of endpoints of the evolving crack may change during the reconstruction. We also mention that, unlike in [41], the endpoints of the crack will not remain fixed during the inversion, and we will need to find an evolution law for these points.

Since we are interested in reconstructing cracks (single or multiples) with finite length completely contained inside of Ω, we introduce a second level-set function ψ in order to select one or more parts from the curve Γ_φ (see Fig. 2).

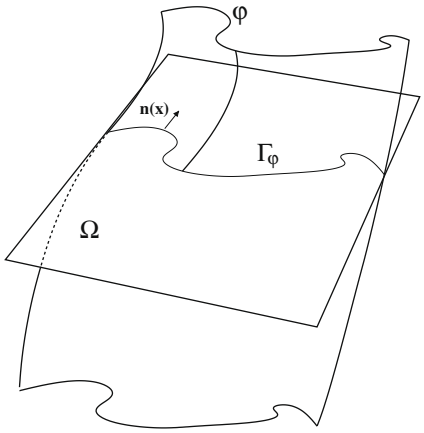

Fig. 1. Modeling of a thin region: first level-set function describing the location and form of the region.

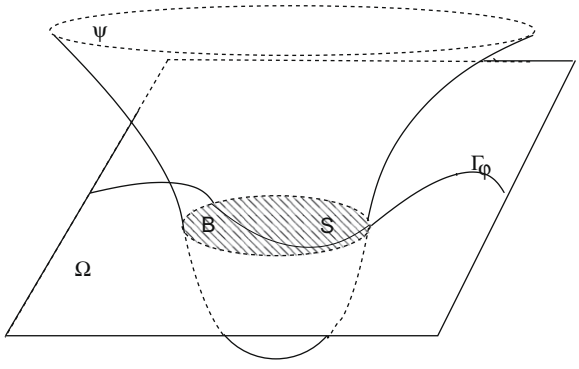

Fig. 2. Modeling of a thin region: second level-set function describing its length and connectivity.

This second level-set function defines the region

$$B = \{(x,y) \in \Omega : \psi(x,y) < 0\}. \tag{5}$$

With this definition we can now specify the cracks as finite sub-intervals of Γ_φ. They are given as

$$S[\varphi,\psi] = \Gamma_\varphi \cap B. \tag{6}$$

In the case of an 'ideal' insulating crack S of thickness zero, Eqs. (1) and (2) have to be supplemented with the null electrical current condition [2]

$$b(\mathbf{x})\frac{\partial u_j}{\partial n} = 0 \quad \text{on } S \tag{7}$$

across the crack.

For further analysis and numerical computation purposes, we will endow the cracks with a small and fixed thickness characterized by $\varepsilon > 0$, and known conductivity b_i much smaller than the background value b_e. For this purpose, we introduce a small neighborhood of Γ_φ, defined by

$$\Gamma_\varphi^\varepsilon = \{\mathbf{y} \in \Omega : \mathbf{y} = \mathbf{x} - \tau\mathbf{n}(\mathbf{x}),\ |\tau| < \varepsilon,\ \mathbf{x} \in \Gamma_\varphi\}. \tag{8}$$

Therefore, we associated the above defined 'ideal crack' S with a 'real crack' counterpart $S_\varepsilon = \Gamma_\varphi^\varepsilon \cap B$, and the insulating condition (7) by the conductivity distribution

$$b(\mathbf{x}) = \begin{cases} b_i & \text{for } \mathbf{x} \in S_\varepsilon \\ b_e & \text{otherwise} \end{cases} \tag{9}$$

in the domain Ω.

3. The inverse problem

3.1. Reconstructing a crack using boundary measurements

Our objective in the inverse problem is to find a (multi) crack which satisfies the measured data, according to some criterion, using a forward model for electrical impedance tomography. The physically measured data, associated to the real conductivity distribution $\tilde{b}(\mathbf{x})$, and taken at positions d_l on the boundary, $l = 1,\ldots,\underline{l}$, are given by

$$\tilde{g}_{jl} = \frac{\partial u_j}{\partial n}(d_l), \tag{10}$$

where u_j solves Eqs. (1) and (2) with (9). We will denote the set of real measurements $\{\tilde{g}_{jl}\}_{l=1,\ldots,\underline{l}}$, for a fixed source j, by $\tilde{g}_j$.

For a guess conductivity distribution $b(\mathbf{x})$, giving simulated measurements g_j, we define the least square cost functional

$$\mathcal{J}_j(b) = \frac{1}{2}\|g_j(b) - \tilde{g}_j\|^2, \tag{11}$$

where $\|\ \|$ represents the usual norm in $\mathbb{R}^{\underline{l}}$.

In our shape-based approach, we will adopt an iterative scheme in which the cost functional (11) is reduced at each step of the reconstruction process. Therefore, we want to find a direction δb such that the cost functional (11) decreases. We assume that $\mathcal{J}_j(b)$ admits the expansion

$$\mathcal{J}_j(b+\delta b) = \mathcal{J}_j(b) + \underbrace{\langle \mathbf{grad}_b \mathcal{J}_j, \delta b\rangle_P}_{\delta\mathcal{J}_j} + O\left(\|\delta b\|_P^2\right) \tag{12}$$

for a sufficiently small variation δb. In (12), $\langle\rangle_P$ represents the canonical inner product in the parameter space, and $\|\ \|_P$ represents the canonical norm. We note that a theoretical proof of the existence of the gradient of $\mathcal{J}_j$ for a parameter distribution b with discontinuities along interfaces are beyond the scope of this paper. We refer to [23,4,18] for more details regarding this issue.

An efficient way to compute the (pixel-based) *gradient direction* of $\mathcal{J}_j$ in b is to use the adjoint formulation [9,33]. We give here the main result.

The gradient direction of $\mathcal{J}_j$ in b is given by

$$\mathbf{grad}_b \mathcal{J}_j = \nabla u_j \cdot \nabla z_j, \tag{13}$$

where u_j solves Eq. (1) and (2) with (9), and z_j solves the following adjoint equation

$$\nabla \cdot b\nabla z_j = 0 \quad \text{in } \Omega, \tag{14}$$

$$bz_j = g_j - \tilde{g}_j \quad \text{on } \partial\Omega. \tag{15}$$

We now want to use this *pixel-based* formulation to define a shape evolution which gradually changes an initial crack into a descent direction until the cost is minimized. The final crack will provide us with the solution of our inverse problem. We note that both the crack and the cost functional (11) depend on the two level-set functions φ and ψ. We will now define descent directions of (11) with respect to these level-set functions. To first order we can write

$$\delta\mathcal{J}_j \approx \delta_\varphi \mathcal{J}_j + \delta_\psi \mathcal{J}_j = \langle \mathbf{grad}_b \mathcal{J}_j, \delta_\varphi b\rangle_P + \langle \mathbf{grad}_b \mathcal{J}_j, \delta_\psi b\rangle_P. \tag{16}$$

In (16), the first term represents the variation due to the deformation of the shape ($\delta_\varphi b$), and the second term represents the variation due to the modification of its length and connectivity ($\delta_\psi b$). We point out that in the direct problem of modeling crack growth, it is assumed that once a part of a crack has formed, that part no longer changes shape or moves [42,43]. Hence, unlike the method present here, in the direct problem of crack growth the zero level set must not be updated behind the crack tips, and therefore, the deformation in the direction normal to the shape is zero when crack growth is modeled.

3.1.1. Deformation of the shape of the crack

In order to simplify the exposition we consider only one source. An analogous result holds for the total cost $\mathcal{J}(b)$, summing up contributions of individual sources γ_j.

To find the change in the cost functional associated to an individual source,

$$\delta_\varphi \mathcal{J}_j = \langle \mathbf{grad}_b \mathcal{J}_j, \delta_\varphi b\rangle_P = \int_\Omega \mathbf{grad}_b \mathcal{J}_j(\mathbf{x})(\delta_\varphi b)dx\,dy, \tag{17}$$

we will follow the line of reasoning given in [39] and will adapt it to our new situation. We denote the boundaries of the extended crack (represented in Fig. 3 with dashed lines) by

$$S^\pm = \{\mathbf{y} \in \Omega : \mathbf{y} = \mathbf{x} \pm \varepsilon \mathbf{n}(\mathbf{x}),\ \mathbf{x} \in S\}. \tag{18}$$

Let us consider an (infinitesimal) displacement $\zeta(\mathbf{x})$ of a point $\mathbf{x} \in S$. Then, $(\delta_\varphi b)$ will make b in the region between S^+ and $(S^+ + \zeta(\mathbf{x}))$ become b_i, and in the region between S^- and $(S^- + \zeta(\mathbf{x}))$ become b_e (see Fig. 3). Note that both incremental areas can be approximated by $\zeta(\mathbf{x})\mathbf{n}(\mathbf{x})ds(\mathbf{x})$, where $ds(\mathbf{x})$ is the incremental arclength. Since $\zeta(\mathbf{x})$ is very small, we can approximate (17) by a line integral,

$$\delta_\varphi \mathcal{J}_j \approx \int_{S^+} (b_i - b_e)\mathbf{grad}_b \mathcal{J}_j(\mathbf{x})\zeta(\mathbf{x})\mathbf{n}(\mathbf{x})ds(\mathbf{x}) - \int_{S^-} (b_i - b_e)\mathbf{grad}_b \mathcal{J}_j(\mathbf{x})\zeta(\mathbf{x})\mathbf{n}(\mathbf{x})ds(\mathbf{x}). \tag{19}$$

This yields

$$\delta_\varphi \mathcal{J}_j = \int_S (b_i - b_e)[\mathbf{grad}_b \mathcal{J}_j|_{S^+} - \mathbf{grad}_b \mathcal{J}_j|_{S^-}]\zeta(\mathbf{x})\mathbf{n}(\mathbf{x})ds(\mathbf{x}), \tag{20}$$

where we have used $\mathbf{grad}_b \mathcal{J}_j|_{S^\pm} = \mathbf{grad}_b \mathcal{J}_j(\mathbf{x} \pm \varepsilon \mathbf{n}(\mathbf{x}))$.

As we can see, if we choose

$$\zeta(\mathbf{x}) = -(b_i - b_e)[\mathbf{grad}_b \mathcal{J}_j|_{S^+} - \mathbf{grad}_b \mathcal{J}_j|_{S^-}]\mathbf{n}(\mathbf{x}) \quad \text{on } S, \tag{21}$$

then the value $\delta_\varphi \mathcal{J}_j$ is negative and, therefore, the cost functional decreases.

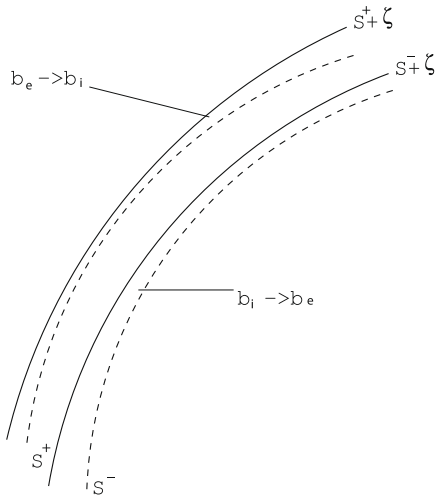

Fig. 3. Variation of conductivity profile due to displacement of crack.

To generate the small displacements $\zeta(\mathbf{x})$ for moving the boundary, we now define on S a velocity function $\mathbf{v}(\mathbf{x}) = F_\varphi(\mathbf{x})\mathbf{n}(\mathbf{x})$, so that

$$\zeta(\mathbf{x}) = F_\varphi(\mathbf{x})\mathbf{n}(\mathbf{x})\tau_\varphi \tag{22}$$

for some small time step τ_φ. This amounts to the movement of points $\mathbf{x} \in S$ by the vector velocity field $\mathbf{v}(\mathbf{x})$. Plugging (22) into (20) we get the descent velocity

$$F_\varphi(\mathbf{x}) = -(b_i - b_e)[\mathbf{grad}_b \mathcal{J}_j|_{S^+} - \mathbf{grad}_b \mathcal{J}_j|_{S^-}] \quad \text{on } S. \tag{23}$$

Letting $\tau \to 0$, and choosing a suitable extension velocity outside S, we now consider the general evolution law [18]

$$\frac{d\varphi}{dt} = F_\varphi(\mathbf{x}) \tag{24}$$

for the level-set function φ. The velocity $F_\varphi(\mathbf{x})$ controls the evolution of the level-set function, and therefore, an appropriate choice is essential in order to obtain an optimal performance of the reconstruction process. We choose to extend the velocity function (23) to all points in the domain as it is discussed in Section 4.3.

A finite difference time discretization of (24) gives us the iteration rule for updating the level-set function at each time step,

$$\varphi^{(n+1)} = \varphi^{(n)} + \tau_\varphi F_\varphi^{(n)}, \varphi^{(0)} = \varphi_0 \tag{25}$$

with step-size $\tau_\varphi > 0$.

3.1.2. Modification of the length and connectivity of the crack

We now want to find descent directions of the second level-set function ψ with respect to the least square cost functional (11). Denote by Γ_ψ the boundary of B, $\Gamma_\psi = \{(x,y) \in \Omega, \psi(x,y) = 0\}$, and by $\mathbf{n}_\psi = \nabla\psi/|\nabla\psi|$ its outward normal. Following the same arguments as in the previous section, we see immediately that a displacement $\mathbf{x} \to \mathbf{x} + \xi(x)\mathbf{n}_\psi(x)$ in the outward normal direction will give rise to a change

$$\delta_\psi \mathcal{J}_j \approx \int_{\Gamma_\psi \cap \Gamma_\psi^\varepsilon} (b_i - b_e)\mathbf{grad}_b \mathcal{J}_j(\mathbf{x})\xi(\mathbf{x})\mathbf{n}_\psi(\mathbf{x})ds(\mathbf{x}). \tag{26}$$

Therefore, the choice of the velocity

$$F_\psi(\mathbf{x}) = -(b_i - b_e)\mathbf{grad}_b \mathcal{J}_j(\mathbf{x})\xi(\mathbf{x})\mathbf{n}_\psi \quad \text{on } \Gamma_\psi \cap \Gamma_\psi^\varepsilon \tag{27}$$

guarantees a descent direction of the cost functional (11).

In fact, in our numerical experiments we will choose the extension velocity such that (27) is applied not only on $\Gamma_\psi \cap \Gamma_\psi^\varepsilon$ but for all points in the domain. In this way, it enables the creation and extinction of objects far away from the actual zero level, enhancing topological changes during the reconstruction. The iteration for the second level set function ψ reads

$$\psi^{(n+1)} = \psi^{(n)} + \tau_\psi F_\psi^{(n)}, \quad \psi^{(0)} = \psi_0. \tag{28}$$

4. Technical details

4.1. Numerical method

To solve the Laplace Eq. (1) in a square domain $\Omega = [0,1] \times [0,1]$ we use finite a element method in a triangular mesh. To this end, we define an uniform square grid of size h and triangulate it by dividing each pixel into two triangles by cutting along one of its diagonals. We implement the applied boundary condition γ_j (source) setting the potential u_j equal 1 on the exterior side of triangle at the position d_j and 0 on the rest of the boundary.

A similar procedure is used to solve the adjoint Eqs. (14) and (15).

4.2. Measurements

To compute the corresponding physical measurements given by (10) and corresponding to the applied potential γ_j, we employ a straightforward finite difference scheme.

In order to avoid the so called 'inverse-crime' we use two different grid sizes for creating the synthetic data and for the reconstruction. To generate the true data we use $h = 1/200$, while for the reconstruction we use $h = 1/100$. In addition, the generated synthetic data $\tilde{g}_j$, associated to the true conductivity distribution $\tilde{b}(\mathbf{x})$, are perturbed by a $\pm 1\%$ of random noise in the following way: $\tilde{g}_j \to \tilde{g}_i(1 + 0.01\Theta_d)$, where Θ_d is an uniform distribution of random numbers between -1 and 1. Therefore, we incorporate to the data a 'systematic noise' component and a 'random noise' component. The resulting data will be denoted by $\{\tilde{g}_{jl}\}_{l=1,\ldots,\underline{l}}$.

4.3. Extension, regularization and smoothing of the descent velocities

The support of the descent velocity functions, as defined in (23) and (27), is not the whole domain Ω, but only a set of measure zero. One possibility to extend these velocities would just be to consider (23) and (27) in larger sets, for example, a small neighborhood of the crack or the whole domain. However, it is well known that the gradient directions computed directly from the adjoint formulation lead to rapidly varying functions in a spatial fine-scale, giving rise to velocities that exhibit strong variations. This introduces instabilities during the reconstruction process that are necessary to avoid. In order to address these issues we choose to extend and smooth the gradient directions by solving the initial value problem for the heat equation

$$\frac{\partial v_{\varphi,\psi}}{\partial t} - \Delta v_{\varphi,\psi} = 0 \quad \text{for } t \in [0,\tau] \tag{29}$$

$$v_{\varphi,\psi}(0) = F_{\varphi,\psi} \tag{30}$$

on Ω, with a prescribe τ and homogeneous Dirichlet boundary conditions. The desired smoothed gradient velocities are then given by

$$\widehat{F}_{\varphi,\psi} = v_{\varphi,\psi}(\tau). \tag{31}$$

Here, the smoothing time τ can be considered as a regularization parameter: for $\tau = 0$ there is no regularization, whereas with increasing τ the updates become increasingly smoothed. Our experience shows that the choice of the value of τ is crucial for the algorithm to succeed. If τ is chosen too small the algorithm does not work well for complicated reconstructions. We choose $\tau = 1$ so that the solutions to Eqs. (29) are sufficiently smooth in the whole domain Ω.

4.4. Reconstruction algorithm

Let us assume that we are given some true data $\{\tilde{g}_{jl}\}_{l=1,\dots,\underline{l}}$. We now outline the reconstruction procedure:

(1) Compute the initial level-set functions, $\varphi^{(0)}(\mathbf{x})$ and $\psi^{(0)}(\mathbf{x})$, corresponding to the initial conductivity profile $b^{(0)}(\mathbf{x})$. We always start with a straight-line crack. Put $n = 0$ and set $j = 1$.
(2) Apply a voltage potential γ_j on the boundary and solve Eqs. (1) and (2) for the forward model on the latest best guess $b^{(n)}[\varphi^{(n)}, \psi^{(n)}]$. This yields the data set $g_j^{(n)} = \{g_{jl}^{(n)}\}_{l=1,\dots,\underline{l}}$.
(3) Compute the residuals $g_j^{(n)} - \tilde{g}_j$, and solve the adjoint problem (14) and (15). Then, the gradient direction of $\mathcal{J}_j$ is given by (13).
(4) Compute the smoothed velocities directions $\widehat{F}_{\varphi,\psi}$ by solving the heat Eq. (29) with prescribe regularization parameters.
(5) Apply the updates (25) and (28) to the level-set functions $\varphi^{(n)}$ and $\psi^{(n)}$, respectively. The step sizes $\tau_\varphi^{(n)}$ and $\tau_\psi^{(n)}$ depend on the activated source γ_j, so the variations provided by each source are similar.
(6) Activate all the sources sequentially. Go to (ii) with $j = j + 1$, until all the voltages have been applied on the boundary. We will refer by an *iteration* of the reconstruction process when all the sources have been used. To avoid certain local minima, we activate the sources on different sides of the domain consecutively in each iteration.
(7) Check the stopping criterion. If it is not satisfied, go to step (ii) with $n = n + 1$ and $j = 1$, and continue from there in an iterative manner.

5. Numerical experiments

In our numerical experiments presented below, we consider a domain $\Omega = [0,1] \times [0,1]$ with uniform background conductivity $b_e = 1$. Inside the domain there is a crack of thickness $\varepsilon = 1/100$ and constant conductivity $b_i = 0.01$. We use 9 sources/detectors equidistantly distributed along each side of the domain. Therefore, $\underline{l} = 9 \times 4$, and each iteration amounts to 36 source activations.

The first experiment consists of a single crack with changing curvature. The results are displayed in a panel of 9 images as shown in Fig. 4. The true crack profile is shown in the center image of the bottom row. We start the reconstruction algorithm with a straight line crack as shown in the top left image. During the first iterations (shown in the center and right images of the top row) the crack looks for its 'right' location, while its length increases rapidily. The images in the middle row show that during the next iterations the crack keeps increasing its length with the right curvature. Notice, that the right curvature at the center of the crack is only achieved at the end of the last iterations. This is so, because the curvature is less sensitive to the measurements than the other key properties of the crack such as its location and length. A comparison between the reconstructed and the real cracks (depicted in the left and center images of the bottom row, respectively) show that the location, length and form of the crack have been reconstructed successfully. In the bottom right image, we have represented, in solid line, the evolution of the cumulative cost associated to one iteration over all different sources, defined by

$$\mathcal{J}_{iter} = \sum_{j=1}^{\underline{l}} \mathcal{J}_j.$$

The noise level is indicated by a dotted line.

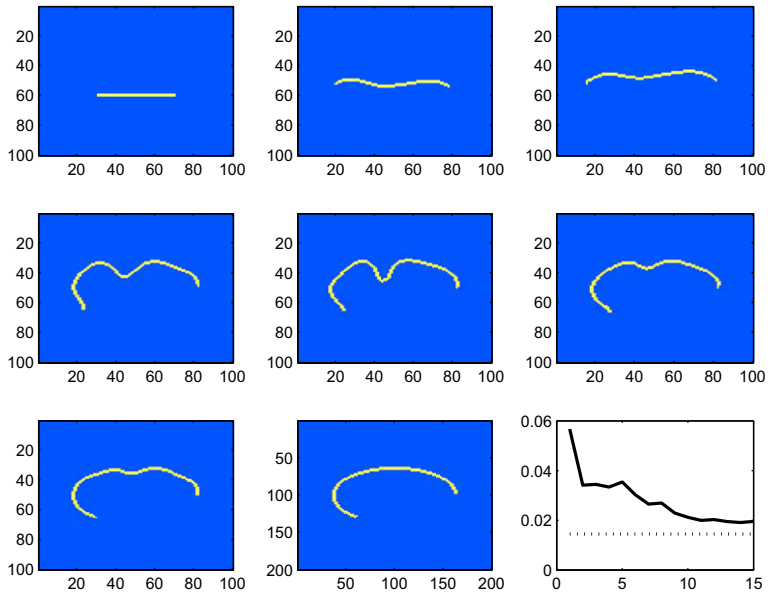

Fig. 4. First numerical experiment: reconstruction of a single crack. Top row (from left to right): Initial profile, profile after 12 source activations (1/3 of the first iteration), and profile after 24 source activations (2/3 of the first iteration). Center row (from left to right): profiles after 4, 7 and 10 iterations. Bottom row (from left to right): Reconstructed profile (after 15 iterations), true profile, and evolution of the cumulative cost J_{iter} versus number of iterations (the noise level is represented with a dotted line).

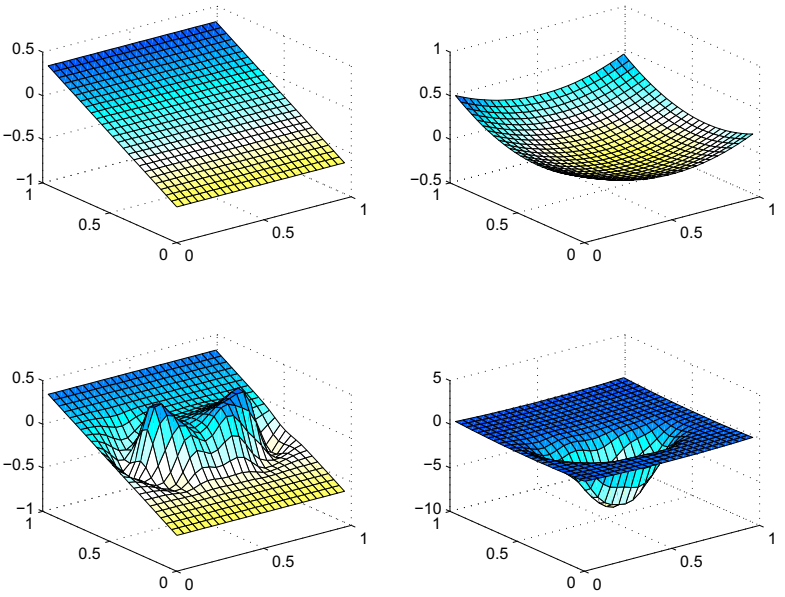

Fig. 5. Initial an final level-set functions for the case presented in Fig. 4. Top row: Initial level-set functions $\varphi^{(0)}(\mathbf{x})$ (left) and $\psi^{(0)}(\mathbf{x})$ (right). Bottom row: Final level-set functions $\varphi^{(15)}(\mathbf{x})$ (left) and $\psi^{(15)}(\mathbf{x})$ (right).

In Fig. 5 we have plotted the initial and final level set functions of the reconstruction process presented above. The top row shows the initial level-set functions $\varphi^{(0)}(\mathbf{x})$ (left image) and $\psi^{(0)}(\mathbf{x})$ (right image). The bottom row shows the final level-set functions $\varphi^{(n)}(\mathbf{x})$ (left image) and $\psi^{(n)}(\mathbf{x})$ (right image) after 15 iterations.

The second experiment deals with the reconstruction of a multi-crack consisting of three disconnected components as shown in the center image of the bottom row of Fig. 6. As in the previous example, the results are displayed in a panel of 9 images that show the profiles at different moments of the reconstruction process (see caption), the true profile (at the center of the bottom row), and the evolution of the cumulative cost along with the noise level. In this example there is not a 'single' location of the true crack, and therefore, during the first iterations the reconstructed crack first breaks into several

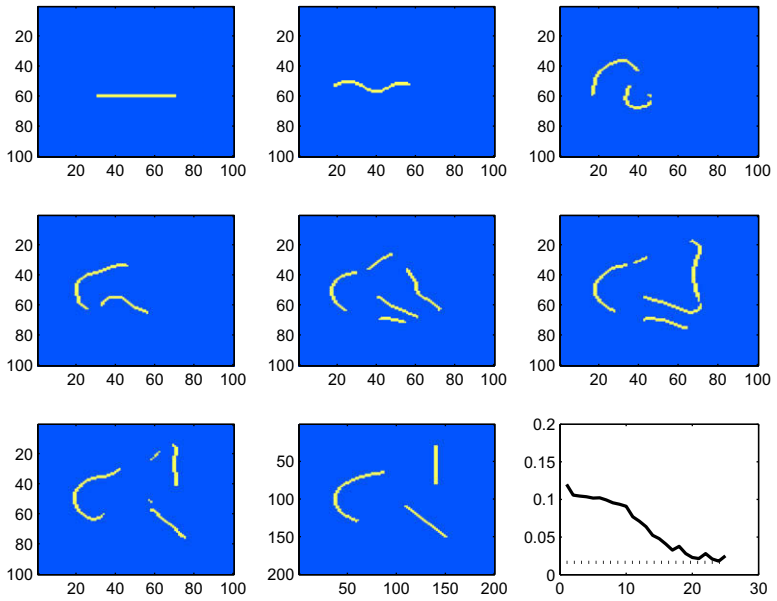

Fig. 6. Second numerical experiment: reconstruction of three cracks. On the two first rows, and from left to right we show: the initial guess, and the reconstructions after 1/3, 1, 7, 10 and 14 iterations. On the third row, and from the left to right we show: the final reconstruction (24 iteration), the real crack, and the evolution of J_{iter} versus the number of iterations (the noise level is represented with a dotted line).

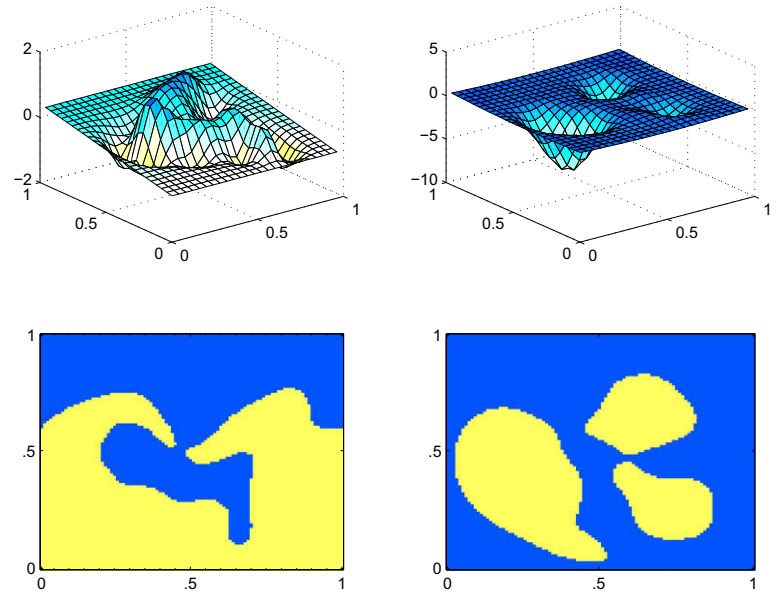

Fig. 7. Top row: Final level-set functions $\varphi^{(24)}(\mathbf{x})$ (left) and $\psi^{(24)}(\mathbf{x})$ (right) of the numerical experiment shown in Fig. 6. Bottom row: contour plot of the sign functions corresponding to $\varphi^{(24)}(\mathbf{x})$ (left) and $\psi^{(24)}(\mathbf{x})$ (right).

pieces. Note that at some intermediate steps of the reconstruction process, there are even more pieces than the true one. At later steps of the reconstruction some of these pieces disappear, and at the end of the iterative process we find the three disconnected shapes of the crack. Again, a comparison between the reconstructed and the real cracks (depicted in the left and center images of the bottom row, respectively) shows a very good estimate of the location, form and connectivity of the real crack.

In the top row of Fig. 7 we have plotted the final level-set functions $\varphi^{(n)}(\mathbf{x})$ (left image) and $\psi^{(n)}(\mathbf{x})$ (right image) of the reconstruction process shown in the previous experiment. The bottom row of this figure shows the corresponding sign func-

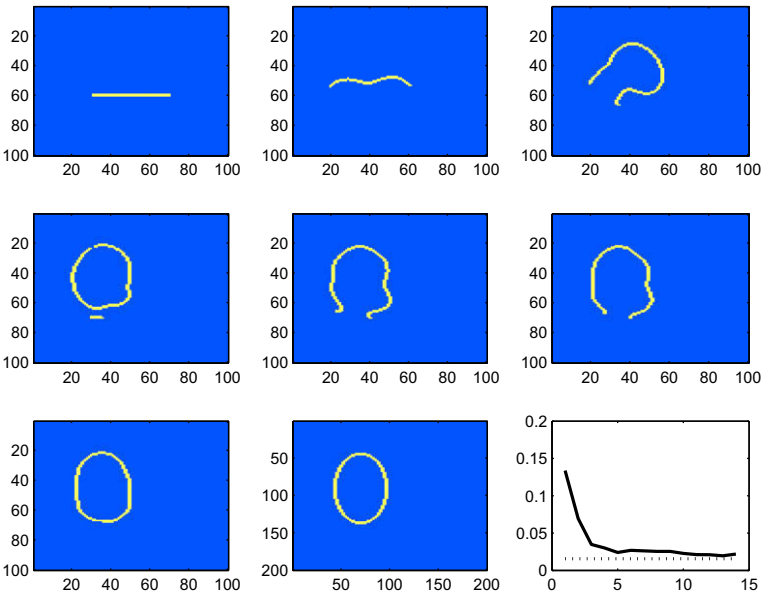

Fig. 8. Third numerical experiment: reconstruction of a close curve. On the two first row, and from left to right we show: the initial guess, and the reconstructions after 1/3, 3/2, 3, 5, 7 iterations. On the third row, and from left to right we show: the final reconstruction (14 iterations), the real crack, and the evolution of J_{iter} versus the number of iterations (the noise level is represented by a dotted line).

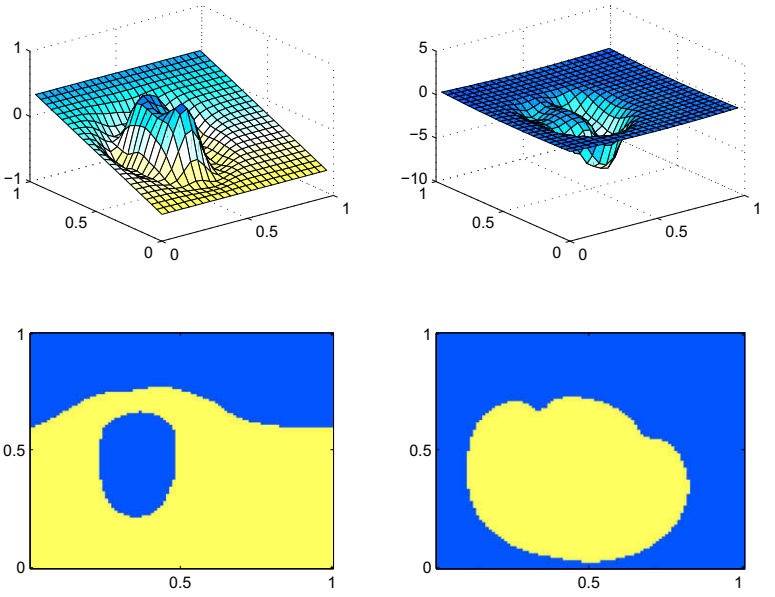

Fig. 9. Top row: Final level-set functions $\varphi^{(14)}(\mathbf{x})$ (left) and $\psi^{(14)}(\mathbf{x})$ (right) of the numerical experiment shown in Fig. 8. Bottom row: contour plot of the sign functions corresponding to $\varphi^{(14)}(\mathbf{x})$ (left) and $\psi^{(14)}(\mathbf{x})$ (right).

tions. Notice, that the intersection between the zero level set of the level-set function φ (bottom left image) and the regions where $\psi < 0$ (bottom right image) defines the reconstructed crack shown in the bottom left image of Fig. 6.

In the third experiment we investigate whether our method is able to reconstruct the shape of a crack represented by a closed curve. Fig. 8 shows the results. From the beginning of the iterative process, the initial guess (left image in the top row) starts bending until it reaches its correct shape (compare the reconstructed and the real cracks depicted in the left and center images of the bottom row, respectively). In Fig. 9, we display the final level set functions (top row) $\varphi^{(n)}(\mathbf{x})$ (left) and $\psi^{(n)}(\mathbf{x})$ (right), and their corresponding sign functions (bottom row). Note that in this case in which the crack consists of a closed curve, the second level-set function $\psi^{(n)}(\mathbf{x})$ on the right column completely encircles the crack defined by the first level-set function $\varphi^{(n)}(\mathbf{x})$ on the left column, and therefore it would not be necessary.

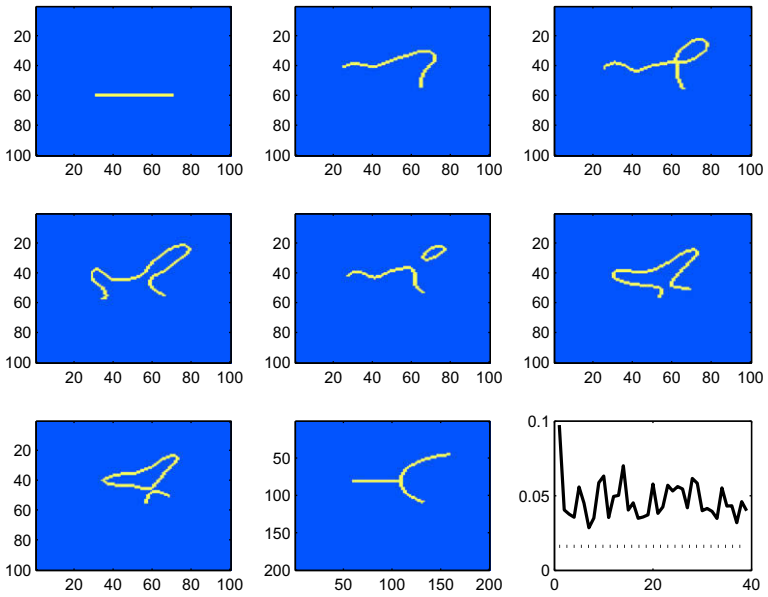

Fig. 10. Fourth numerical experiment: a pitchfork shape. On the two first row from the left to right: initial guess, and reconstruction after 2, 4, 10, 15 and 27 iterations. On the third row from the left to right: final reconstruction (40 iterations), real crack and evolution of J_{iter} versus the number of iter (the noise level is represented by a dotted line).

Finally, we show the results for the case in which the crack has a pitchfork shape, as shown in the center image of the bottom row in Fig. 10. In this case there is a singular point from which three crack branches depart. The cost, depicted in the right bottom image, shows a rapid decrease during the first few iterations of the reconstruction. When the reconstructed crack is located nearby the real crack, although with a wrong shape (see the center image of the top row), the cost reaches a local minimum. The following iterations of the reconstruction process exhibit an oscillatory behavior of the cost evolution. This is so, because in each step of the algorithm we force the reconstructed crack to move a certain number of pixels, even-though it could be in a local minimum (observe that in the previous reconstructions the cost functional is not strictly decreasing neither). We note that during the reconstruction, our algorithm creates branches that are removed at the next iterations in a non convergent way. Nevertheless, we point out that the reconstructions associated with the global minima of the cost function (shown, for example, in the center images of the top and middle rows) allow us to estimate the location and length of the real crack and to guess its real shape.

6. Conclusions

We have extended the usual level-set technique for modeling and propagating volumetric objects to the case of very thin objects such as cracks. For this purpose, two level-set functions have been employed in this work: one to model the location and shape of the crack, and the other to define its length and connectivity. A shape-based reconstruction technique, such as the one presented here, performs particulary well in the cases where there is some noticeable contrast between the object and the background medium, so the interfaces are well defined. This is especially important in the applications in which it is more important to recover the shapes of the hidden objects than to recover their internal properties.

In this work, we have demonstrated that our approach gives rise to good reconstructions in the presence of noise, even for quite difficult situations. So far, we have limited our investigation to the case in which the electrical properties are piecewise constant over the whole domain with only two possible values that are known a priori. In our future research, we plan to investigate more complicated situations in which we will simultaneously reconstruct the shape and the conductivity value in the interior of the crack.

Acknowledgments

The authors acknowledge support from the Spanish Ministry of Education and Science (Grant No. FOS2007-62673) and by the Autonomous Region of Madrid (Grant No. S-0505/ENE/0229, COMLIMAMS).

References

[1] J.F.P.J. Abascal, M. Lambert, D. Lesselier, O. Dorn, 3-D Eddy-current imaging of metal tubes by gradient-based, controlled evolution of level sets, IEEE Trans. Magn. 44 (12) (2008) 4721–4729.

[2] A. Ben Abda, M. Kallel, Line segment crack recovery from incomplete boundary data, Inverse Probl. 18 (2002) 1057–1077.
[3] S. Andrieux, A. Ben Abda, H.D. Bui, Reciprocity principle and crack identification, Inverse Probl. 15 (1999) 59–65.
[4] G. Bal, K. Ren, Reconstruction of singular surfaces by shape sensitivity analysis and level set method, Math. Models Meth. Appl. Sci 16 (8) (2006) 1347–1373.
[5] L. Baratchart, J. Leblonde, F. Mandré, E.B. Saff, How can the meromorphic approximation help to solve some 2D inverse problems for the Laplacian?, Inverse Probl 15 (1999) 79–90.
[6] Z. Belhachmi, D. Bucur, Stability and uniqueness for the crack identification problem, SIAM J. Control Optim. 46 (2007) 253–273.
[7] E. Beretta, E. Francini, Asymptotic formulas for perturbations of the electromagnetic fields in the presence of thin imperfections, Contemp. Math. 333 (2003) 49–63.
[8] L. Borcea, J.G. Berryman, G. Papanicolaou, High contrast impedance tomography, Inverse Probl. 12 (1996) 935–958.
[9] L. Borcea, Electrical impedance tomography, topical review, Inverse Probl. 18 (2002) R99–R136.
[10] M. Brühl, M. Hanke, M. Pidcock, Crack detection using electrostatic measurements, Math. Model. Numer. Anal. 35 (2001) 595–605.
[11] P. Burchard, L.T. Cheng, B. Merriman, S. Osher, Motion of curves in three spatial dimensions using a level set approach, J. Comput. Phys. 170 (2001) 720–741.
[12] M. Burger, A level set method for inverse problems, Inverse Probl. 17 (2001) 1327–1355.
[13] F. Cakoni, D. Colton, The sampling method for cracks, Inverse Probl. 19 (2003) 279–295.
[14] Y. Capdeboscq, M.S. Vogelius, Imagerie électromagntique de petites inhomogénitiés, ESAIM: Proc. 22 (2008) 40–51.
[15] M. Cheney M, D. Isaacson, J.C. Newell, Electrical impedance tomography, SIAM Rev. 40 (1999) 85–101.
[16] D.L. Chopp, N. Sukumar, Fatigue crack propagation of multiple coplanar cracks with extended finite element/fast marching method, Int. J. Eng. Sci. 41 (2003) 845–869.
[17] O. Dorn, E. Miller, C. Rappaport, A shape reconstruction method for electromagnetic tomography using adjoint fields and level sets, Inverse Probl. 16 (2000) 1119–1156.
[18] O. Dorn, D. Lesselier, Level set methods for inverse scattering, Inverse Probl. 22 (2006) R67–R131.
[19] A.R. Elcrat, V. Isakov, O. Neculoiu, On finding a surface crack from boundary measurements, Inverse Probl. 11 (1995) 343–351.
[20] M. Duflot, A study of the representation of cracks with level sets, Int. J. Numer. Meth. Eng. 70 (2007) 1261–1302.
[21] H. Feng, W.C. Karl, D. Castanon, Tomographic reconstruction using curve evolution, in: Proc. IEEE Int. Conf. Computer Vision Pattern Recognition, Hilton Head Island, 13–15 June 2000, vol. 1, 2000, pp. 361–366.
[22] A. Friedman, M. Vogelius, Determining cracks by boundary measurements, Indiana Univ. Math. J 38 (1989) 527–556.
[23] F. Hettlich, Frechet derivatives in inverse obstacle scattering, Inverse Probl. 11 (1995) 371–382.
[24] D. Holder, Clinical and Physiological Application of Electrical Impedance Tomography, UCL Press, London, 1993.
[25] K. Ito, K. Kunisch, Z. Li, Level-set approach to an inverse interface problem, Inverse Probl. 17 (2001) 1225–1242.
[26] A. Kirsch, S. Ritter, A linear sampling method for inverse scattering from an open arc, Inverse Probl. 16 (2000) 89–105.
[27] R. Kress, Inverse scattering from an open arc, Math. Meth. Appl. Sci. 18 (1995) 267–293.
[28] R. Kress, Inverse elastic scattering from a crack, Inverse Probl. 12 (1996) 667–684.
[29] R. Kress, P.A. Serranho, A hybrid method for two-dimensional crack reconstruction, Inverse Probl. 21 (2005) 773–784.
[30] V. Liepa, F. Santosa, M. Vogelius, Crack determination from boundary measurements – reconstruction using experimental data, J. Nondestruct. Evaluat. 12 (1993) 163–174.
[31] A. Litman, D. Lesselier, D. Santosa, Reconstruction of a two-dimensional binary obstacle by controlled evolution of a level-set, Inverse Probl. 14 (1998) 685–706.
[32] M. McIver, An inverse problem in electromagnetic crack detection, IMA J. Appl. Math. 47 (1991) 127–145.
[33] F. Natterer, F. Wübbeling, Mathematical Methods in Image Reconstruction, Monographs on Mathematical Modeling and Computation, Vol. 5, SIAM, Philadelphia, 2001.
[34] S. Osher, J.A. Sethian, Fronts propagating with curvature-dependent speed: algorithms based on Hamilton–Jacobi formulations, J. Comput. Phys. 79 (1988) 12–49.
[35] S. Osher, R. Fedkiw, Level Set Methods and Dynamic Implicit Surfaces, Springer, New York, 2003.
[36] W.K. Park, Diffraction Inverse par des Inclusions Minces et des Fissures, Doctorate Thesis, École Polytechnique, Palaiseau, 2009.
[37] C. Ramananjaona, M. Lambert, D. Lesselier, J-P. Zolésio, Shape reconstruction of buried obstacles by controlled evolution of a level set: from a min–max formulation to numerical experimentation, Inverse Probl. 17 (2001) 1087–1111.
[38] L. Rondi, A variational approach to the reconstruction of cracks by boundary measurements, J. Math. Pures Appl. 87 (2007) 324–342.
[39] F. Santosa, A level set approach for inverse problems involving obstacles, ESAIM Control, Optim. Calc. Variat. 1 (1996) 17–33.
[40] J.A. Sethian, Level Set Methods and Fast Marching Methods, second ed., Cambridge Univ. Press, Cambridge, 1999.
[41] P. Smereka, Spiral crystal growth, Physica D 138 (2000) 282–301.
[42] M. Stolarska, D.L. Chopp, N. Moës, T. Belytschko, Modelling crack growth by level sets in the extended finite element method, Int. J. Numer. Meth. Eng. 51 (2001) 943–960.
[43] M. Stolarska, D.L. Chopp, Modelling thermal fatigue cracking in integrated circuits by level sets and the extended finite element method, Int. J. Eng. Sci. 41 (2003) 2381–2410.
[44] G. Ventura, J.X. Xu, T. Belytschko, A vector level set method and new discontinuity approximations for crack growth by EFG, Int. J. Numer. Meth. Eng. 54 (2003) 923–944.